



HAL
open science

Diving into micro-and macroscopic properties of eggtempera paint based on Sienna pigment

Floriane Gerony, Côme Thillaye Du Boullay, Laurence de Viguerie, Fabrice Gaslain, Bruno Lanson, Camille Colin, Laurent Michot, Anne-Laure Rollet, Guillaume Mériguet, Maguy Jaber

► To cite this version:

Floriane Gerony, Côme Thillaye Du Boullay, Laurence de Viguerie, Fabrice Gaslain, Bruno Lanson, et al.. Diving into micro-and macroscopic properties of eggtempera paint based on Sienna pigment. Applied Clay Science, 2024, 249, pp.107236. 10.1016/j.clay.2023.107236 . hal-04443938

HAL Id: hal-04443938

<https://hal.science/hal-04443938v1>

Submitted on 7 Feb 2024

HAL is a multi-disciplinary open access archive for the deposit and dissemination of scientific research documents, whether they are published or not. The documents may come from teaching and research institutions in France or abroad, or from public or private research centers.

L'archive ouverte pluridisciplinaire **HAL**, est destinée au dépôt et à la diffusion de documents scientifiques de niveau recherche, publiés ou non, émanant des établissements d'enseignement et de recherche français ou étrangers, des laboratoires publics ou privés.

Diving into micro-and macroscopic properties of egg-tempera paint based on Sienna pigment

Floriane Gerony^{a,b}, Laurence de Viguerie^a, Côme Thillaye du Boullay^a, Fabrice Gaslain^c, Bruno Lanson^d, Camille Colin^a, Laurent Michot^b, Anne-Laure Rollet^b, Guillaume Mériquet^b, Maguy Jaber^{a,e*}

^a Sorbonne Université, CNRS UMR 8220, LAMS, case courrier 225, 4 pl. Jussieu 75252 Paris cedex 05, France

^b Sorbonne Université, CNRS UMR 8234, PHENIX, case courrier 51, 4 pl. Jussieu 75252 Paris cedex 05, France

^c MinesParis, UniversitéPSL, CentredesMatériaux(MAT), UMR7633 CNRS, 91003 Evry, France

^d Univ. Grenoble Alpes, CNRS, Univ. Savoie Mont Blanc, IRD, Univ. Gustave Eiffel, ISTERre, F-38000 Grenoble, France

^e Institut Universitaire de France, Paris, France

*Corresponding author, e-mail: maguy.jaber@sorbonne-universite.fr

Abstract

Egg-tempera painting was a pictorial technique widespread in the Middle Ages. In this work, Sienna earth and yolk have been used to formulate tempera paints according to historical recipes. Micro- and macroscopic properties were investigated to understand the interactions between the pigment and the binder. The pigment, inorganic part of the paint, was characterized by X-Ray Diffraction (XRD), thermal analysis (TG-DTA), Fourier Transform Infrared (FT-IR) Spectroscopy, granulometry, as well as Scanning Electron Microscopy (SEM). Then lecithin adsorption onto pigment particles was probed to understand yolk interaction with Sienna earth, pure kaolinite and goethite particles. NMR-Relaxometry was used to investigate the behavior and accessibility of the mineral surfaces to yolk and water. Macroscopic rheological properties of the paint systems were finally investigated.

Keywords: tempera paint; Sienna earth; yolk; lecithin; relaxometry; rheology

Introduction

Until the end of the 15th century, the predominant painting technique was *tempera*, *i.e.* a mixture of a colored pigment with an aqueous binder. In Western Europe, between the 13th and 15th centuries, the most commonly used aqueous binder was egg yolk and many artists therefore painted with an egg-tempera technique. Some tempera binder recipes are reported in medieval manuscripts.

32 For instance, in the famous manuscript “Libro Del Arte”, the apprentice painter Cennino Cennini (1390-
33 1437) described the mixing of egg yolk and pigments, and mentioned that such a mixture could be
34 used to paint a wide range of materials : walls, panels, or iron among others (Cennini and Broecke,
35 2015). Numerous pigments both synthetic and natural were employed by artists at that time. Among
36 them, as mentioned in several medieval manuscripts (Mayer and Sheehan, 1991; Merrifield, 1999;
37 Clarke, 2011; Cennini and Broecke, 2015), natural earths and ochres were particularly popular, as
38 they were used to form the base of the first paint layers of flesh tones. Sienna earth is a typical
39 example of this family of pigments. Most of these pigments are complex mineral mixtures. Sienna
40 earth mainly contains goethite, various clay minerals (kaolinite, smectite, illite...), and additional
41 accessory minerals, the nature of which depends on the geological setting (Helwig, 1998; Grygar et
42 al., 2003; Hradil et al., 2003).

43 Identification techniques classically used on tempera artworks and mock-ups do not provide
44 any information about the interactions between pigments and binders, even though these interactions
45 are of prime importance since they govern the final properties of the paints. Still, some spectroscopic
46 analyses have been carried out in mock-ups after drying (Meilunas et al., 1990; Mazzeo et al., 2008;
47 Navas et al., 2010; Romero-Pastor et al., 2011; Manea et al., 2012). In the case of egg-tempera paint
48 with Sienna, some interactions between the pigments and egg yolk could be evidenced from the
49 spectral evolution of the aliphatic and aromatic C-H regions of aromatic amino acids (Romero-Pastor
50 et al., 2011). Fanost and coworkers studied green earth tempera paints (Fanost, 2019; Fanost et al.,
51 2022) and showed that the combination of NMR-relaxometry and rheology measurements on fresh
52 paints provides fruitful information on the binder-pigment network that controls to a large extent the
53 rheological properties of paints and consequently the way they flow and spread on canvases (Salvant
54 Plisson et al., 2014) which often explains why painters chose specific formulations.

55 The present paper deals with egg-tempera painting with Sienna earth as pigment. After characterizing
56 in details the structural and morphological properties of Sienna by various techniques (XRD, FTIR,
57 Laser diffraction, Gas adsorption, Thermo Gravimetric Analysis, Scanning Electron Microscopy), we
58 focused on the interactions between the pigment and the binder, analyzing the adsorption of lecithin,
59 one of the main components of egg yolk, on the pigments and probing interfaces between binder and
60 pigment with NMR relaxometry. Sienna earth being a complex natural system, we also investigated
61 the possibility to use a mixture of pure minerals as a synthetic Sienna. The rheological properties of

62 natural Sienna tempera paint were then compared to the ones of tempera paints based on the
63 reconstituted Sienna as well as its individual components. Model systems are often employed in
64 physicochemical studies but, to the best of our knowledge, it is the first use of a model pigment in the
65 cultural heritage field.

66 Materials and methods

67 Materials

68 Italian raw Sienna (#40400) and synthetic goethite (#48000, purity >99.4%) were supplied by Kremer
69 Pigmente (Germany). Clay minerals kaolinite (KGa-1b, purity kaolin 95-100%, quartz 1-2%) and
70 montmorillonite (Texas STx-1, purity montmorillonite 95-100%, quartz 1-5%) were purchased from The
71 Clay Minerals Society (USA). Calcite (purity >99%) was obtained from Sigma-Aldrich.

72 Reconstituted Sienna is the mix of the pure minerals with proportions by weight of 37% kaolinite, 27%
73 goethite, 14% montmorillonite and 22% calcite.

74 Fresh organic hen eggs were purchased from a local store.

75 Soybean L- α -Lecithin (CAS 8002-43-5 – Calbiochem®) was obtained from Sigma-Aldrich and was
76 solubilized in ethanol denatured $\geq 96\%$ (CAS 64-17-5, GPR RECTAPUR®) from VWR BDH Chemicals.

77 The headgroup area of lecithin ($a_0 = 0.58 \text{ nm}^2$) was determined with Avogadro software (Version
78 1.2.0) using Universal Force Field (UFF) and is consistent with literature values (Brouillette et al.,
79 1982; Israelachvili, 2011).

80

81 Sample preparation

82 Adsorption isotherms

83 As lecithin is not soluble in water, it was solubilized into ethanol. 20 mL of lecithin/ethanol solutions (at
84 concentrations in the range 2-100 mM for Sienna and kaolinite and 2-350 mM for goethite) were
85 added to 300 mg of powder in closed flasks and stirred for 24h. Dispersions were then centrifuged at
86 4000 *g* during 15 min. Solid substrates were analyzed by thermogravimetric analysis coupled with
87 differential thermal analysis (TG-DTA) to determine the charge *Q* (mass of lecithin adsorbed per gram
88 of powder). For Sienna and goethite isotherms, lecithin charge was not directly measurable by TGA
89 analysis because lecithin decomposition and goethite to hematite transition occur in the same

90 temperature range (Figure 2 and Figure S2). We estimated the loss of weight due to iron oxides
91 transformation and the remaining loss of weight was assigned to lecithin decomposition.

92 Paint reconstruction protocol

93 Paints were formulated after selecting recipes from medieval manuscripts and more recent manuals
94 (Laurie, 1926; Thompson and York, 1962; De L'escalopier, 1977; Mayer and Sheehan, 1991;
95 Merrifield, 1999; Clarke, 2011; Cennini and Broecke, 2015) and further discussion with restorers. A
96 simplified preparation protocol was elaborated to be applicable and reproducible in the laboratory.
97 Pure yolk was obtained by rolling the yolk from one hand to another to remove the white, and by
98 piercing the yolk to eliminate the membrane (Mayer and Sheehan, 1991). In order to improve
99 reproducibility, 3 fresh organic hen egg yolks from the same box were mixed. Tempera binder was
100 prepared by mixing egg yolk (75 wt%) with ultra-pure water (25 wt%).

101 For rheology measurements, tempera paints were prepared as follows: 3 g of pigment were manually
102 ground into 2 g of ultra-pure water during 2 min with a glass muller. Then 4 g of tempera binder were
103 added to the pigment paste and mixed again with the glass muller during 4 min. In the end, paint
104 systems correspond to $\frac{1}{3}$ pigment, $\frac{1}{3}$ water and $\frac{1}{3}$ egg yolk.

105 For relaxometry measurements, $\frac{1}{3}$ of pigment was dispersed in water or in tempera binder and ground
106 with a glass muller.

107 Analytical techniques

108 X-ray diffraction (XRD) and Rietveld refinement

109 XRD patterns were collected on natural Sienna using a Bruker D8 diffractometer equipped with Co
110 radiation ($\lambda = 1.78897 \text{ \AA}$) operated at 40 kV and 40 mA. Intensities were measured with a Vortex 60EX
111 silicon drift detector (Hitachi High-Tech America) for 8 s per 0.026° 2θ step over the $5\text{--}90^\circ$ 2θ Co K α
112 angular range. Divergence slit, the two Soller slits, the antiscatter, and resolution slits were fixed at
113 0.3° , 2.3° , 0.3° , and 0.2° , respectively. Quantitative phase analysis was performed from the Rietveld
114 refinement of XRD data using the Profex software (Doebelin and Kleeberg, 2015). Quantification of the
115 sample amorphous content was also performed from the Rietveld refinement of XRD data after
116 addition of an internal standard (~ 20 wt% of corundum – $\alpha\text{-Al}_2\text{O}_3$) to the sample and careful mixing
117 and homogenization.

118 Scanning electron microscopy (SEM)

119 Analyses were carried out with a FEI Nova NanoSEM 450 microscope equipped with a FEG source
120 and an immersion lens. Secondary electron imaging was performed with a through-the-lens detector
121 (TLD) between 2 and 5 kV.

122 Laser diffraction particle size analyser

123 Size measurements were performed with a Mastersizer 3000 laser diffraction particle size analyzer
124 with Hydro EV accessory (Malvern Panalytical). Powders were dispersed in water. 3 measurements
125 were made per sample and the values are reported as volume and number distributions.

126 Gas adsorption

127 N₂ adsorption-desorption isotherms of natural Sienna and goethite were carried out at 77 K on a
128 Micromeritics ASAP 2010 gas analyzer. Prior to the analysis, the samples were outgassed under
129 vacuum at 200°C for 6 h. Specific surface areas were determined using the BET model.

130 Thermogravimetric Analysis (TGA)

131 Thermal analyses were performed with a SDT-Q600 (TA Instruments). Approximately 20 mg of
132 powder were placed in an alumina crucible and a temperature ramp of 5°C/min was applied from 25 to
133 1000°C. Measurements were conducted with an air flow of 75 mL/min.

134 NMR-Relaxometry

135 Measurements of the water ¹H longitudinal relaxation rates $R_1=1/T_1$ were performed using a
136 SpinMaster Field Cycling relaxometer (Stelar) in the 0.01-30 MHz frequency range. From 10 kHz to 10
137 MHz a pre-polarized sequence was used whereas a non-polarized sequence was employed between
138 10 MHz and 30 MHz (Anoardo et al., 2001). The magnetization curves, built with 16-time increments,
139 exhibit a mono-exponential dependency. Samples were conditioned in glass tubes (10 mm external
140 diameter, 38 mm length) closed by a silicon cap (Fanost et al., 2020). 30wt% suspensions of mineral
141 were prepared by grinding the powder in a water with a glass muller. For calcite suspension, which is
142 not very stable, measurements were taken point by point and samples were shaken between each
143 measurement. The sample almost completely filled the tube to prevent evaporation during the
144 experiments. Samples were thermostated at 298 K using regulated air flux.

145 FT-IR spectroscopy

146 Fourier-transform infrared (FT-IR) spectra were acquired on a Bruker Tensor 27 spectrometer.
147 Transmission measurements were performed using KBr (CAS 7758-02-3 – Uvasol®, for IR
148 spectroscopy, Merck, Germany) transparent pellets that were obtained by applying a weight of 10 tons
149 on mixtures of about 2 mg of powder and 100 mg of anhydrous KBr previously crushed and
150 homogenized in an agate mortar. A 32-scan average spectrum was recorded from 4000 to 400 cm⁻¹
151 with a resolution of 4 cm⁻¹. Baseline subtraction and peak indexation were performed using OriginPro
152 9.0 software.

153 Rheology

154 Rheological measurements were carried out using a Thermo Scientific HAAKE MARS 40 rheometer. A
155 sandblasted titanium 35 mm-diameter and 2°-angle cone/plate geometry was used. Tests were
156 performed at 25°C using a plastic hood to avoid drying of the paint during the measurements. All tests
157 were carried out at least twice on the same paint and on the same day. Error bars were computed as
158 the standard deviation of these measurements.

159 Flow measurements were performed by increasing and decreasing the shear rate between $\dot{\gamma} = 0.01$
160 and 1000 s⁻¹. Because back and forth measurements were almost superimposed (i.e. thixotropic
161 effects are negligible), only the downward ramp is plotted in the following; exception for kaolinite where
162 the upward ramp is shown because the low viscosity of the suspension caused sedimentation during
163 the measurement.

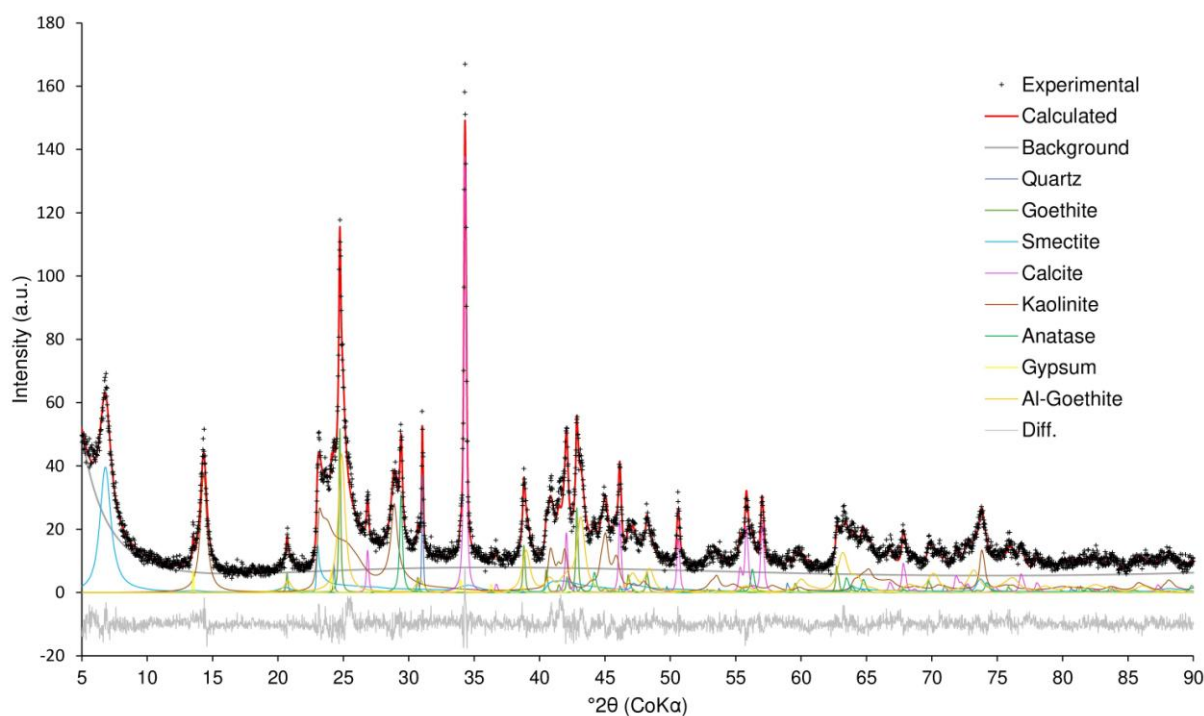
164 Strain sweep measurements were performed at increasing stresses from $\tau = 0.01$ to 100 Pa at a
165 constant oscillatory frequency of 1 Hz.

166 Frequency sweep measurements were carried out at constant stress $\tau = 0.1$ Pa (value chosen in the
167 linear viscoelastic regime) with decreasing frequency from 100 to 0.1 Hz.

168 Results and discussion

169 Natural Sienna characterization and reconstruction:

170 The X-ray diffraction pattern of natural Sienna (Figure 1) reveals the presence of numerous mineral
171 phases, the relative proportions of which were deduced from a Rietveld refinement of XRD data (Table
172 1).



173

174 *Figure 1: Rietveld refinement results (experimental pattern in black, calculated pattern in red, difference in grey) of natural*
 175 *Sienna. Rp = 7.77%, Rwp = 10.12%, Rexp = 8.41%, GoF = 1.20.*

176 Natural Sienna is mainly composed of clay minerals (~33% kaolinite and ~12% smectite) and iron
 177 oxide (~24% goethite). A significant amount of calcite (~13%) is also present in the pigment. The
 178 systematic presence of broad and sharp lines corresponding to goethite (Figure S1) indicated the
 179 coexistence of two goethite populations in natural Sienna. Positions of sharp lines are typical of ideal
 180 goethite whereas broad lines are systematically shifted towards higher angle (Figure S1) most likely
 181 owing to common Al-for-Fe substitutions in goethite (Schulze, 1984; Schwertmann and Cornell, 2000).
 182 The associated decrease of volume unit cell (from 0.1387 nm³ in ideal goethite to 0.1366 nm³ in Al-
 183 substituted goethite) indicates the presence of 10-15 mol% Al in the prevailing (~75% of the total
 184 goethite content in natural Sienna) Al-substituted goethite (Schwertmann and Carlson, 1994). Peak
 185 broadening associated to Al-for-Fe substitution in goethite indicates a decrease of the average
 186 coherent scattering domain size from ~80 nm to ~15 nm.

187 *Table 1: Quantitative phase analysis of natural Sienna determined by Rietveld refinement.*

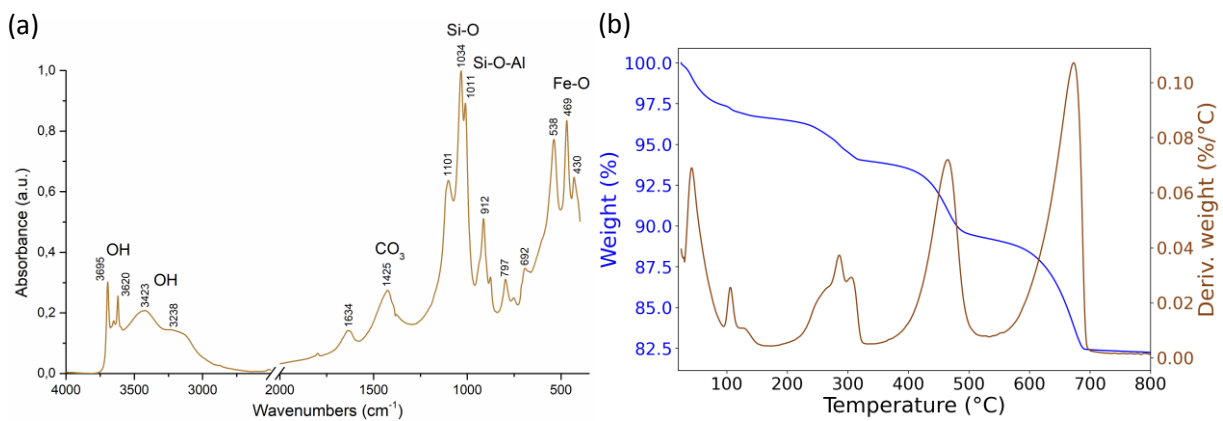
Minerals	%wt
Kaolinite	32.7(5)
Goethite	23.5(4)
Calcite	12.9(2)
Smectite	12.1(5)
Anatase	2.7(1)

Quartz	1.6(1)
Gypsum	0.7(1)
Amorphous	13.8(11)

188

189 The IR spectrum of natural Sienna is presented in Figure 2a. Vibration bands corresponding to
 190 kaolinite, goethite and calcite can be identified in this spectrum. The presence of kaolinite is evidenced
 191 by the Si-O stretching band at 1034 cm^{-1} and the Si-O-Al band at 1011 cm^{-1} . The two OH stretching
 192 bands at 3695 and 3620 cm^{-1} that correspond to structural hydroxyls can also be linked to the
 193 presence of kaolinite. Bands corresponding to goethite are also observed particularly in the low
 194 wavenumber region where signals at 538 , 469 and 430 cm^{-1} correspond to Fe-O, in addition of those
 195 at 3423 and 3238 cm^{-1} assigned to the hydroxyl groups. However, the latter bands could also be
 196 related to the presence of smectite. Finally, the presence of calcite in the sample is evidenced by the
 197 occurrence of the carbonate stretching vibration band at 1425 cm^{-1} (Helwig, 1998; Bikiaris et al., 2000;
 198 Genestar and Pons, 2005; Manasse and Mellini, 2006).

199 The TG-DTA curve of natural Sienna (Figure 2b) displays various weight losses. The features below
 200 150°C can be assigned to the outgassing of physisorbed water. The event around 285°C corresponds
 201 to the goethite/hematite transition (Manasse and Mellini, 2006). In quantitative terms, this event
 202 corresponds to a weight loss of 2.5% of the initial mass. The weight loss for pure goethite would
 203 correspond to 10%, leading to an estimation of 25% of goethite in natural Sienna, a value extremely
 204 close to the one deduced from the Rietveld refinement. The weight losses around 465°C and 675°C
 205 can be assigned to respectively kaolinite dehydroxylation and calcite decomposition (Genestar Juliá
 206 and Pons Bonafé, 2004). There again the quantitative results are consistent with mineral proportions
 207 deduced from the Rietveld analysis.

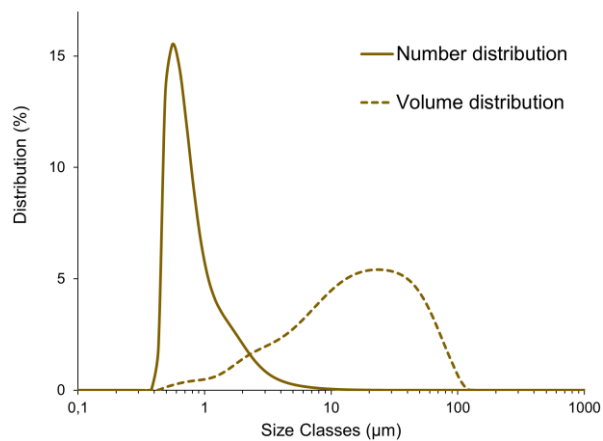


208

209

Figure 2 : (a) Transmission infrared spectrum of natural Sienna in the region $4000\text{-}400\text{ cm}^{-1}$. (b) TG-DTA curves of Sienna.

210 The particle size distribution of Sienna was determined by laser diffraction (Figure 3). The volume
211 distribution (dashed line) exhibits a wide range of sizes and is centered around 25 μm . However, such
212 a representation of the results tends to favor the larger particles and it is relevant to plot the number
213 distribution (solid line). This shows that most particles in Sienna are submicronic in size with a
214 distribution centered around 1 μm . It must be recalled however that laser diffraction results assume
215 the presence of spherical objects, which is obviously not the case here as shown by SEM images
216 (Figure 4). The sizes determined should then be considered as indicative rather than a precise value.

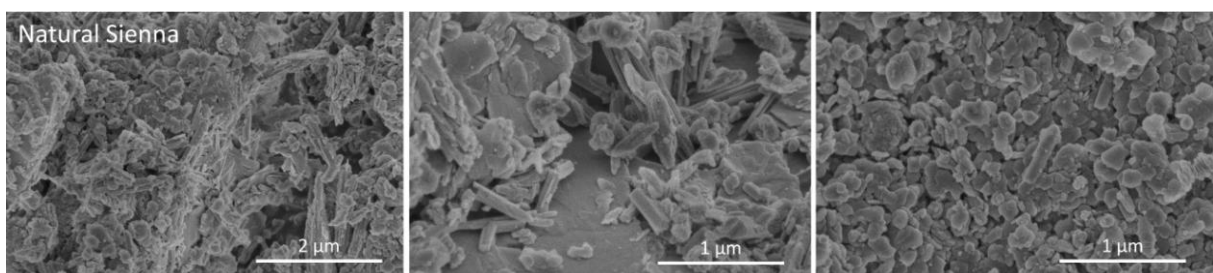


217
218

Figure 3: Size distribution in volume and in number of Sienna particles in water.

219 Scanning Electron Microscopy (SEM) micrographs of natural Sienna (Figure 4) reveal two main crystal
220 morphologies. Indeed, platy particles and needle-like ones can be observed. EDX analyses (not
221 shown) reveal that the platy particles contain mainly silicon, aluminum and/or calcium whereas the
222 needle-like ones are iron-rich. It then appears that the platelets can be assigned to clay minerals and
223 the needles to goethite. In terms of size, the goethite particles are about 1 μm long and 0.1 μm wide
224 whereas the platelets have a diameter (d) of about 100 nm and a thickness (e) of about 20 nm, i.e. an
225 aspect ratio d/e of 0.2. Literature reports that natural Sienna can contain low amounts of manganese
226 oxide, giving it a brownish hue (Hradil et al., 2003), and that arsenic is sometimes present in Sienna
227 samples (Manasse and Mellini, 2006). These two elements were not observed in the Sienna used in
228 the present study.

229

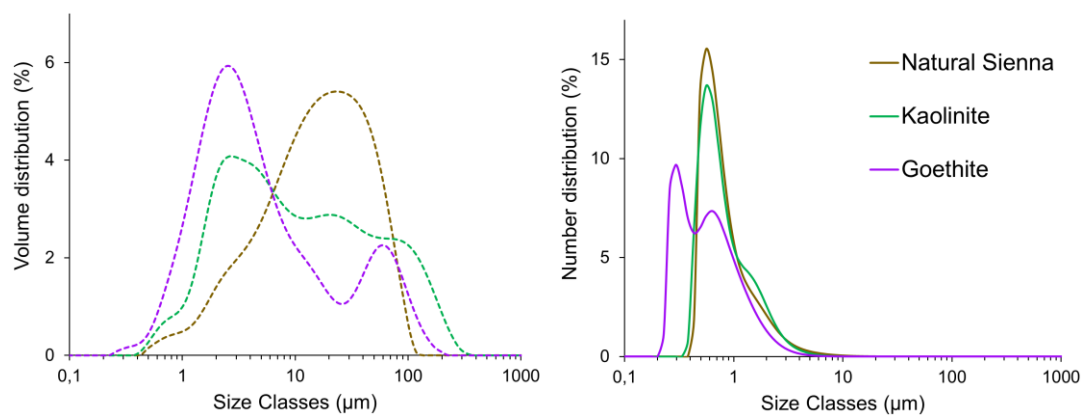


230

Figure 4: SEM photos of natural Sienna.

231 The specific surface area (SSA) of natural Sienna determined by gas adsorption is $45.8 \text{ m}^2 \cdot \text{g}^{-1}$, a large
232 value that appears consistent with the submicron size of most particles deduced from SEM images
233 and laser diffraction results.

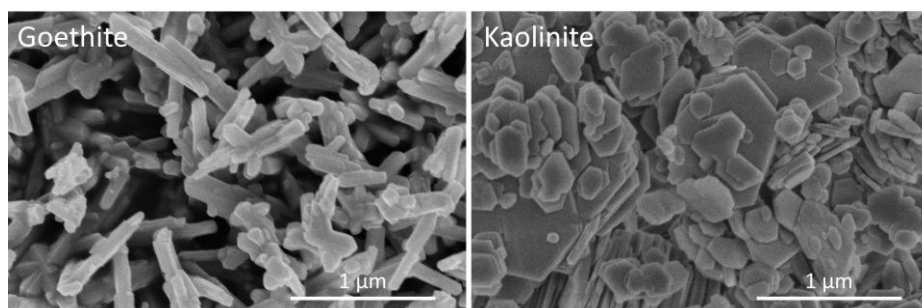
234 Sizes and morphological properties of pure goethite and pure kaolinite later used as model systems in
235 this study have also been characterized. Size measurements of both minerals are compared to those
236 obtained for natural Sienna in Figure 5. The range of sizes of both goethite and kaolinite is similar to
237 that of natural Sienna, most particles being submicronic (Figure 5 right).



238

239 Figure 5: Size distribution in volume (left) and in number (right) of particles in Sienna (brown curve), pure kaolinite (green curve)
240 and pure goethite (purple curve) in water.

241 SEM images of pure minerals goethite and kaolinite are presented on Figure 6. The shape and size of
242 goethite particles are similar to those of the needle-like grains observed in natural Sienna (about $1 \mu\text{m}$
243 $\times 0.1 \mu\text{m}$), whereas the pure kaolinite appears to be formed of slightly larger particles (about $1 \mu\text{m}$ in
244 the layer plane for the largest) than those observed in natural Sienna.



245

246

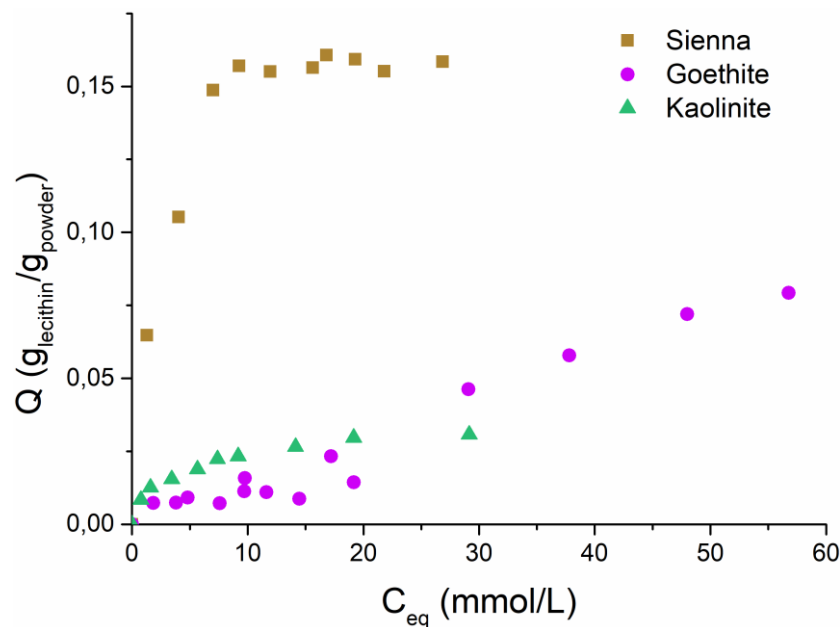
Figure 6: SEM photos of pure goethite and pure kaolinite.

247 The specific surface area of pure goethite was measured as $14.7 \text{ m}^2 \cdot \text{g}^{-1}$ and the SSA of pure kaolinite
248 is reported by the supplier as $10.1 \text{ m}^2 \cdot \text{g}^{-1}$, whereas for STx-1 montmorillonite a SSA of $83.8 \text{ m}^2 \cdot \text{g}^{-1}$ is
249 indicated.

250 At first sight, in terms of morphological features, pure kaolinite and pure goethite thus appear as
251 proper models for understanding the properties of natural Sienna employed as pigment in tempera
252 paint.

253 Adsorption of the binder on the pigment

254 In order to get more insight into the effect of binder in egg yolk-based tempera paints, it seems
255 relevant to examine the adsorption of binder molecules onto pigment particles. Egg yolk is mainly
256 composed of water (around 50%), lipids (around 30%), and proteins (around 15%). The remaining 5%
257 correspond to carbohydrates, minerals, colored molecules and vitamins (Phenix, 1997; Anton, 2007,
258 2013; Xiao et al., 2020). The main phospholipid present in yolk, phosphatidylcholine, generally
259 referred to as lecithin accounts for 12% of dry matter of yolk (Phenix, 1997). We therefore chose in a
260 first step to use lecithin and studied its adsorption onto natural Sienna and some of its component
261 minerals.



262
263 *Figure 7: Adsorption isotherms of lecithin on natural Sienna (brown squares), on goethite (purple circles) and on kaolinite (green*
264 *triangles): evolution of the adsorbed charge of lecithin Q in function of the equilibrium concentration of lecithin C_{eq} .*

265 The isotherm adsorption of lecithin on natural Sienna (brown squares in Figure 7) exhibits a sharp
266 increase at low equilibrium concentration followed by a plateau at $Q_{\text{Sienna}} = 0.16 \text{ g/g}$ for lecithin
267 concentration $> 10 \text{ mmol/L}$. Such a shape is indicative of a high affinity of lecithin towards Sienna
268 earth. Looking at the individual components, it appears that the isotherm corresponding to kaolinite
269 displays a similar shape with a plateau around $Q_{\text{kaolinite}} = 0.03 \text{ g/g}$ (green triangles in Figure 7),
270 whereas the isotherm for goethite exhibits a low adsorbed amount at low equilibrium concentration
271 followed by a steady increase of the amount adsorbed. This latter result is rather surprising, as
272 goethite is known to have a strong affinity towards phosphate groups (Chitrakar et al., 2006; Luengo et
273 al., 2006; Zhong et al., 2007), even in natural materials (Torrent, 1992). However, when looking at the
274 structure of lecithin, it appears that the phosphate groups in lecithin may not be easily accessible since
275 the phosphate is bound to a choline and a glycerol moieties. Furthermore, lecithin is positively charged
276 on the choline group (Li et al., 2023), which could explain its low affinity for goethite that has an
277 isoelectric point around 7.0. Still, adsorption isotherms here were carried out in ethanol and ~~that~~ such
278 reasoning may not fully apply.

279 All these results tend to show that lecithin adsorption on natural Sienna is likely dominated by
280 adsorption onto clay fractions. Such an interpretation is reinforced by the fact that the specific surface
281 area ratio between pure kaolinite ($\approx 10 \text{ m}^2 \cdot \text{g}^{-1}$) and natural Sienna ($\approx 50 \text{ m}^2 \cdot \text{g}^{-1}$) is very close to the
282 adsorbed amount ratio of lecithin between the two systems. Furthermore, the shape of the adsorption
283 isotherm with a plateau highlights saturation of the adsorbed lecithin charge. Considering a surface
284 headgroup of the lecithin molecule of 0.58 nm^2 , the saturation value corresponds to the charge of
285 almost two layers of lecithin molecules absorbed on Sienna and kaolinite. This would suggest a bilayer
286 adsorption, which has been reported in the literature for intercalation between bentonite sheets (Li et
287 al., 2023).". Still, it is rather difficult to obtain a full quantitative picture of lecithin adsorption on natural
288 Sienna considering that the surface areas of the various components in the complex system is not
289 known. Moreover, goethite in natural Sienna is not equivalent to the pure goethite used in our study.
290 Indeed, detailed analysis of the diffractogram have shown that most of the goethite present in natural
291 Sienna earth was in fact microcrystalline Al-substituted goethite (Figure S1).

292 Solvent accessibility to mineral: NMR relaxometry

293 As presented above, Sienna earth is composed of several minerals, whose precise chemical
294 composition and proportions vary according to their provenance. We thus decided to prepare a

295 synthetic Sienna by mixing pure minerals (goethite, kaolinite, montmorillonite and calcite) in
296 proportions similar to those determined from the Rietveld refinement of natural Sienna (Table 1) and to
297 compare their behavior as paints, as well as those of the individual minerals. For montmorillonite, we
298 chose to use the STx-1 sample from the Clay Minerals Society as it is a classical representative of a
299 Ca^{2+} exchanged montmorillonite. Amorphous phases were replaced by calcite.

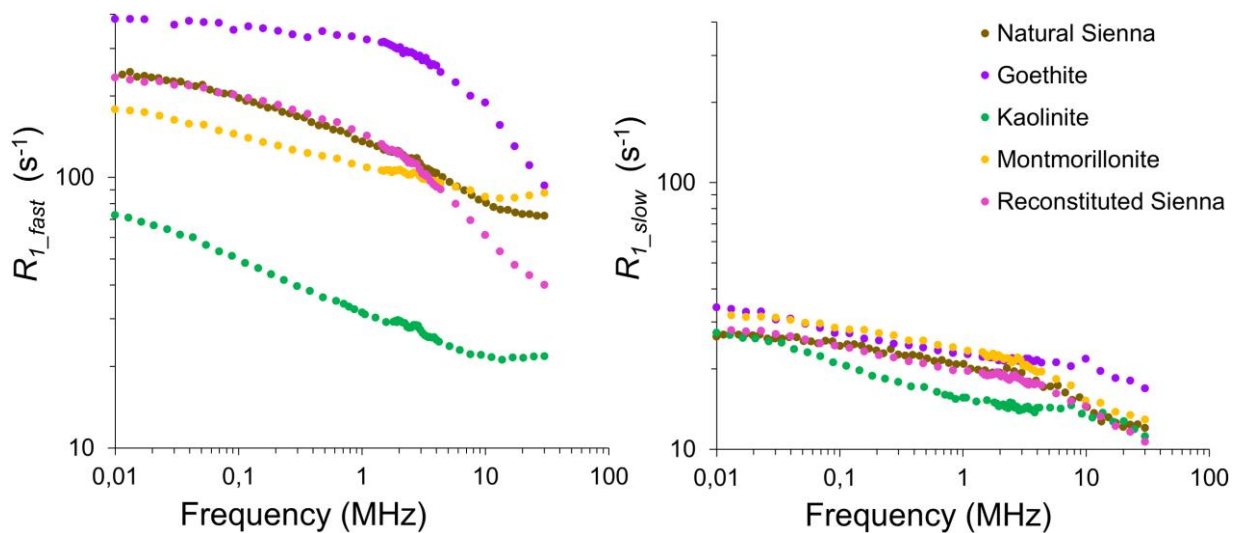
300 An important feature to understand paint behavior is to assess the proportion of pigment
301 surfaces that are actually accessible to solvent molecules, i.e. in this case mainly water and lipoprotein
302 molecules. NMR relaxometry is a perfectly suited tool for probing such phenomena as it provides
303 information on the multiscale dynamics of molecules (Kimmich, 1997; Korb, 2018). In particular,
304 measuring the NMR relaxation rate $R_1=1/T_1$ of ^1H at Larmor frequency spanning from 0.01 to 30 MHz,
305 provide insights into the dynamics of water and lipoproteins in the vicinity of mineral surfaces, and into
306 their interactions with surface atoms (Cooper et al., 2013; Yuan et al., 2017; Fanost et al., 2021).

307 Figure 8 shows the ^1H NMR relaxation dispersion (NMRD) profiles of tempera paints pigmented with
308 the main mineral components of Sienna (goethite, kaolinite, montmorillonite), and of both natural and
309 reconstituted Sienna earths. The relaxation rate R_1 at each frequency is determined by the fitting of
310 the magnetization curves by exponential decays. Here, two populations of protons have been
311 identified, a fast relaxation rate named R_{1_fast} and a slow one named R_{1_slow} . The profiles of the fast
312 population of the five minerals differ from each other. Peaks are visible at 2-4 MHz corresponding to
313 ^1H - ^{14}N quadrupolar peaks (Kimmich, 1977; Fanost et al., 2022) assessing the presence of poorly
314 mobile proteins. Conversely, R_{1_slow} curves are similar for all mineral components. Quadrupolar peaks
315 are also present assessing the presence of more mobile proteins. R_{1_fast} represent 70% of the signal
316 relaxation and R_{1_slow} the remaining 30% which is close to the proportions respectively of water ^1H and
317 of lipoproteins ^1H contained in the tempera binder. Consequently, R_{1_fast} can be attributed to the
318 relaxation rates of water ^1H in the vicinity of proteins and R_{1_slow} to the lipoproteins ^1H .

319 To go further in the understanding of the interactions between the solvent and the pigment, NMRD
320 profiles of aqueous dispersions of the mineral components have been recorded without egg yolk
321 (Figure S5). Similarly to Fanost et al. (2022), magnetization curves have mono-exponential
322 dependence. The shape of the NMRD profiles of aqueous dispersions is very similar to the R_{1_fast}
323 curves (corresponding to interactions with water ^1H) in tempera dispersions. This is a strong
324 confirmation that R_{1_fast} corresponds to water in the vicinity of mineral in the tempera paint. Again, the

325 different suspensions display significantly different NMRD profiles that seem to be mineral-specific, as
326 reported by Fanost et al. (2021) in the case of green earth pigments. The curve corresponding to
327 goethite is the one that exhibits the highest R_1 values over the whole frequency range. This is linked to
328 the presence in this sample of high amounts of paramagnetic species, mainly Fe(III). The more Fe(III)
329 is present in a mineral, the higher its R_1 value (Helm, 2006). Furthermore, in the case of goethite, the
330 magnetic moment of Fe(III) are aligned yielding to a super magnetic moment with a strong magnetic
331 anisotropy (magnetic moment blocked on the structural axis of the particle) (Mørup et al., 1983;
332 Dekkers, 1989; Bocquet et al., 1992). The NMRD profile of goethite (Figure 8 and Figure S5) is
333 characteristic of such magnetic particles. Curves corresponding to clay minerals, i.e. kaolinite and
334 montmorillonite display a significantly different shape with a smooth and steady decreases of R_1 with
335 frequency. Furthermore, the profile corresponding to montmorillonite is located at higher R_1 values
336 than that of kaolinite. Such a difference can be assigned to the difference in surface area between
337 those two phyllosilicates. Indeed, R_1 is sensitive to the amount of surface accessible to water (the
338 higher the surface, the higher R_1).

339 In multicomponent systems, the NMRD profiles of a suspension formed with a mixture of minerals is
 340 equal to the sum of the NMRD profiles of each component weighted by its proportion in the mixture
 341 (Fanost et al., 2021). This is indeed the case for the profile of the reconstituted Sienna up to 3 MHz.
 342 Comparing the latter with that of natural Sienna, both profiles are almost superimposed at low
 343 frequencies. This is even more evident considering the NMRD profiles in tempera binder (Figure 8).
 344 However, for frequencies higher than 3 MHz, a marked difference in shape can be observed. Indeed,
 345 the R_1 curve corresponding to natural Sienna exhibit a slighter decrease of R_1 at high frequency than
 346 reconstituted Sienna which shows a goethite-like shape. Such a difference could be assigned to a
 347 non-accessibility of water to goethite in the natural sample but, in view of the morphological features
 348 described above, this appears rather unlikely. Another explanation could be found in the crystal-
 349 chemistry of goethite revealed by X-ray diffraction, most of which being Al-substituted. Such crystal
 350 chemistry significantly decreases the amount of structural paramagnetic atoms, which could explain
 351 the observed difference in profile shapes (Figure 8 and Figure S5). In any case, this shows that
 352 defining proper model systems able to reproduce natural samples requires a thorough mineralogical,
 353 crystal-chemical, and morphological characterization of the natural samples as subtle variations in
 354 crystal chemistry or texture may have a significant impact on some properties.



356 *Figure 8: Relaxation rates (R_1) for tempera paints. Left: R_{1_fast} and right: R_{1_slow} , obtained from biexponential fit of the*
 357 *magnetization decays.*

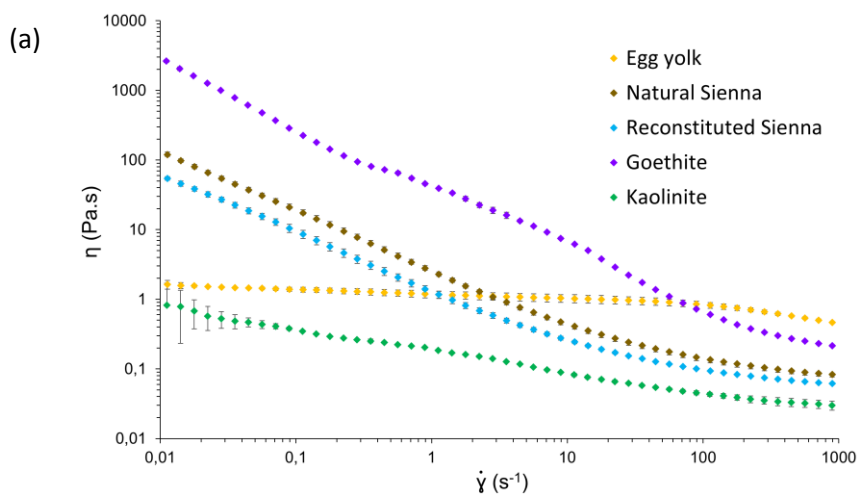
358 Formulation of tempera paints: effect of the mineral on rheological properties of 359 paints

360 Rheological properties give insights into the consistency and texture of paints from low
361 sollicitation to high deformation, corresponding to the flow under the painter's brush. Tempera paints
362 prepared with natural Sienna are stable in time as no significant sedimentation is observed during the
363 time of use, which may be due to swelling clays present in natural Sienna, such as montmorillonite.
364 Figure 9a displays the flow curves of tempera prepared with kaolinite and goethite, and those of both
365 natural and reconstituted Siennas. The flow curve of pure egg yolk is also plotted as a reference. Egg
366 yolk exhibits a low viscosity ($\approx 1 \text{ Pa s}$) and a moderate shear thinning in agreement with previous
367 studies (Fanost, 2019). Kaolinite and goethite-based tempera formulae both display a much more
368 pronounced shear thinning behavior. For the same mass fraction, and despite a lower volume fraction,
369 goethite suspension exhibits a viscosity much higher than that of the kaolinite suspension. This
370 difference may be due to the differences in size and shape between both samples (Mueller et al.,
371 2010; Puisto et al., 2012), goethite being smaller and more anisotropic (Figure 5 and Figure 6).
372 Tempera paints based on both natural and reconstituted Siennas exhibit a flow behavior intermediate
373 between those of their two main components, i.e. kaolinite and goethite. Furthermore, the viscosity of
374 the natural sample is slightly higher than that of its reconstituted counterpart, which can be due to the
375 higher specific surface area of natural Sienna that possibly allows for more interactions between the
376 pigment and the binder. It is worth pointing out the fact that shear thinning is a required property for
377 industrial paints, and can therefore be a feature of interest for artists. Indeed, for low shear rates, a
378 high viscosity is needed to prevent settling and dripping after application, while for shear rates
379 between 100 and 1000 s^{-1} , corresponding to the shear rates exerted by a painter's brush, the viscosity
380 should be low enough to allow easy flow and spreading (Larson et al., 2022). Dynamic oscillatory
381 measurements confirm a different behavior between pure binder and paint formulations (Figure 9b and
382 10c). The strain sweep measurements of pure egg yolk (Figure 9b) reveal a liquid-like behavior
383 whatever the applied strain with a viscous modulus (G'') higher than the elastic one (G'). Conversely,
384 at low strain (from 0.1 to 1%), tempera paints prepared with both natural and reconstituted Siennas
385 display viscoelastic properties with G' values significantly higher than G'' . The Linear Visco-Elastic
386 Region (LVER) extends up to strains of 1% . G' and G'' intersect at the critical strain (for $\gamma \approx 20\%$),
387 which is a characteristic behavior of suspension pastes and a feature common to numerous paint

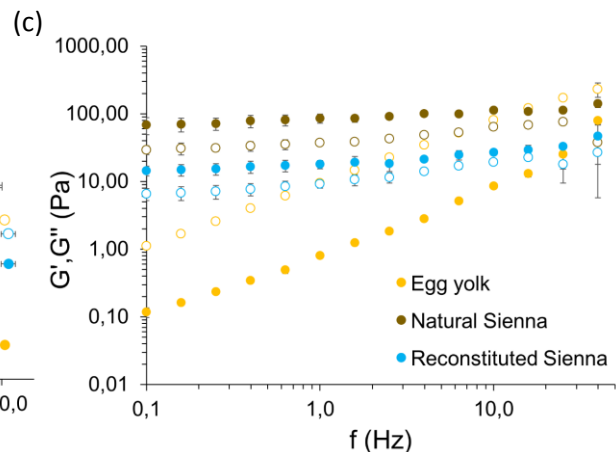
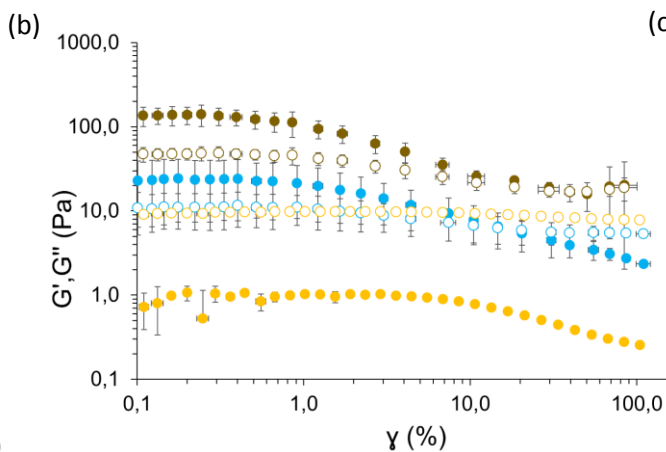
388 formulations (Salvant Plisson et al., 2014). In agreement with flow measurements, for the same
 389 volume fraction, the elastic and viscous moduli of formulae based on natural Sienna are slightly higher
 390 than those of the reconstituted sample.

391 Frequency sweep measurements (Figure 9c) were carried out in the LVER for an applied stress of 0.1
 392 Pa, i.e. a strain of $\gamma \approx 0.1\%$. Whereas both G' and G'' increase with frequency for pure egg yolk, the
 393 curves corresponding to natural and reconstituted Sienna samples exhibit constant G' and G'' values
 394 independent of the applied frequency, which tends to a gel-like behavior. All these experiments
 395 suggest that the main rheological features of tempera based on natural Sienna are well captured by
 396 using a model system, despite the imperfection of the present one.

397



398



399

400 *Figure 9: Rheological measurements of egg yolk and tempera paints with natural Sienna and reconstituted Sienna. For*
 401 *comparison with pure minerals, flow measurements of paint preparations with goethite and kaolinite are plotted. Flow*
 402 *measurements (a), strain sweep (b) and frequency sweep (c). G' in full circles and G'' in empty circles. Error bars for 2*
 403 *measurements of the same paint.*

404 CONCLUSION

405 This paper proposes a detailed investigation of egg-tempera paint based on Sienna earth, a very
406 common pigment of complex composition, focusing first on the pigment composition, then probing its
407 physico-chemical properties in interaction with the binder. Different systems were monitored,
408 considering either historical reconstructions (natural Sienna earth and egg yolk), simplified model
409 systems (with lecithin and a synthetic Sienna earth) or even the pure components of the pigment.
410 Interactions between lecithin and Sienna or its main constituents were studied. The high amount of the
411 surfactant adsorbed on Sienna compared to kaolinite and goethite highlighted probably the synergy
412 between all minerals constituting natural Sienna. Relaxation rates measured on the different minerals
413 in water pointed out that Sienna is a complex microstructure that cannot result from a simple physical
414 mix of pure minerals, even though the rheological properties might suggest the opposite. Due to the
415 complexity of modelling the behavior of tempera paint, the relevance of the models proposed depends
416 on the scale of the properties studied: for macroscopic properties, it seems that reconstituted Sienna
417 fits well with the natural one while at the mesoscopic scale, systems should be chosen carefully. All in
418 all, the composition of the pigment is of great importance while mixing with the binder, allowing the
419 artist to give the desired texture to its paint based on rheological properties.

420

421

422

423

424 Bibliography

- 425 Anoardo, E., Galli, G., Ferrante, G., 2001. Fast-field-cycling NMR: Applications and instrumentation.
426 *Appl. Magn. Reson.* 20, 365–404. <https://doi.org/10.1007/BF03162287>
- 427 Anton, M., 2013. Egg yolk: structures, functionalities and processes: Egg yolk: structures,
428 functionalities and processes. *J. Sci. Food Agric.* 93, 2871–2880.
429 <https://doi.org/10.1002/jsfa.6247>
- 430 Anton, M., 2007. Composition and Structure of Hen Egg Yolk, in: Huopalahti, R., López-Fandiño, R.,
431 Anton, M., Schade, R. (Eds) *Bioactive Egg Compounds*. Berlin, pp. 1–6.
- 432 Bikiaris, D., Daniilia, S., Sotiropoulou, S., Katsimbiri, O., Pavlidou, E., Moutsatsou, A.P., Chrysoulakis,
433 Y., 2000. Ochre-differentiation through micro-Raman and micro-FTIR spectroscopies:
434 application on wall paintings at Meteora and Mount Athos, Greece. *Spectrochim. Acta. A.*
435 *Mol. Biomol. Spectrosc.* 56, 3–18. [https://doi.org/10.1016/S1386-1425\(99\)00134-1](https://doi.org/10.1016/S1386-1425(99)00134-1)
- 436 Bocquet, S., Pollard, R.J., Cashion, J.D., 1992. Dynamic magnetic phenomena in fine-particle goethite.
437 *Phys. Rev. B* 46, 11657–11664. <https://doi.org/10.1103/PhysRevB.46.11657>

438 Brouillette, C.G., Segrest, J.P., Ng, T.C., Jones, J.L., 1982. Minimal size phosphatidylcholine vesicles:
439 effects of radius of curvature on head group packing and conformation. *Biochemistry* 21,
440 4569–4575. <https://doi.org/10.1021/bi00262a009>

441 Cennini, C., Broecke, L., 2015. Cennino Cennini's *Il libro dell'arte*: a new English translation and
442 commentary with Italian transcription. Archetype Publications, London.

443 Chitrakar, R., Tezuka, S., Sonoda, A., Sakane, K., Ooi, K., Hirotsu, T., 2006. Phosphate adsorption on
444 synthetic goethite and akaganeite. *J. Colloid Interface Sci.* 298, 602–608.
445 <https://doi.org/10.1016/j.jcis.2005.12.054>

446 Clarke, M., 2011. *Mediaeval painters' materials and techniques: the Montpellier Liber diversarum*
447 *arcium*. Archetype, London.

448 Cooper, C.L., Cosgrove, T., van Duijneveldt, J.S., Murray, M., Prescott, S.W., 2013. The use of solvent
449 relaxation NMR to study colloidal suspensions. *Soft Matter* 9, 7211.
450 <https://doi.org/10.1039/c3sm51067k>

451 De L'escalopier, C., 1977. Théophile Prêtre et Moine, *Essai Sur Divers Arts*, Libr. des Arts et métiers-
452 Ed. J. Laget. ed.

453 Dekkers, M.J., 1989. Magnetic Properties of Natural Goethite-I. Grain-Size Dependence of Some Low-
454 and High-Field Related Rockmagnetic Parameters Measured At Room Temperature.
455 *Geophys. J. Int.* 97, 323–340. <https://doi.org/10.1111/j.1365-246X.1989.tb00504.x>

456 Doebelin, N., Kleeberg, R., 2015. Profex: a graphical user interface for the Rietveld refinement
457 program BGMN. *J. Appl. Crystallogr.* 48, 1573–1580.
458 <https://doi.org/10.1107/S1600576715014685>

459 Fanost, A., 2019. *Formulation et propriétés physico-chimiques de peintures a tempera à base de*
460 *jaune d'œuf et de terres vertes* (Ph.D. dissertation). Sorbonne Université, Paris.

461 Fanost, A., de Viguerie, L., Ducouret, G., Mériquet, G., Walter, P., Glanville, H., Rollet, A.-L., Jaber, M.,
462 2022. Connecting Rheological Properties and Molecular Dynamics of Egg-Tempera Paints
463 based on Egg Yolk. *Angew. Chem. Int. Ed.* 61, e202112108.
464 <https://doi.org/10.1002/anie.202112108>

465 Fanost, A., Jaber, M., de Viguerie, L., Korb, J.-P., Levitz, P.E., Michot, L.J., Mériquet, G., Rollet, A.-L.,
466 2021. Green earth pigments dispersions: Water dynamics at the interfaces. *J. Colloid*
467 *Interface Sci.* 581, 644–655. <https://doi.org/10.1016/j.jcis.2020.07.085>

468 Fanost, A., Jaber, M., de Viguerie, L., Korb, J.-P., Levitz, P.E., Michot, L.J., Mériquet, G., Rollet, A.-L.,
469 2020. Green Earth pigments aqueous dispersions: NMR relaxation rates dataset. *Data Brief*
470 32, 106270. <https://doi.org/10.1016/j.dib.2020.106270>

471 Genestar, C., Pons, C., 2005. Earth pigments in painting: characterisation and differentiation by
472 means of FTIR spectroscopy and SEM-EDS microanalysis. *Anal. Bioanal. Chem.* 382, 269–274.
473 <https://doi.org/10.1007/s00216-005-3085-8>

474 Genestar Juliá, C., Pons Bonafé, C., 2004. The use of natural earths in picture: study and
475 differentiation by thermal analysis. *Thermochim. Acta* 413, 185–192.
476 <https://doi.org/10.1016/j.tca.2003.10.016>

477 Grygar, T., Hradilová, J., Hradil, D., Bezdička, P., Bakardjieva, S., 2003. Analysis of earthy pigments in
478 grounds of Baroque paintings. *Anal. Bioanal. Chem.* 375, 1154–1160.
479 <https://doi.org/10.1007/s00216-002-1708-x>

480 Helm, L., 2006. Relaxivity in paramagnetic systems: Theory and mechanisms. *Prog. Nucl. Magn.*
481 *Reson. Spectrosc.* 49, 45–64. <https://doi.org/10.1016/j.pnmrs.2006.03.003>

482 Helwig, K., 1998. The characterisation of iron earth pigments using infrared spectroscopy. IRUG² VA
483 Postprints 83–92.

484 Hradil, D., Grygar, T., Hradilová, J., Bezdička, P., 2003. Clay and iron oxide pigments in the history of
485 painting. *Appl. Clay Sci.* 22, 223–236. [https://doi.org/10.1016/S0169-1317\(03\)00076-0](https://doi.org/10.1016/S0169-1317(03)00076-0)

486 Israelachvili, J.N., 2011. *Intermolecular and surface forces*, 3rd ed. ed. Academic press, Burlington
487 (Mass.).

488 Kimmich, R., 1997. *NMR*. Springer Berlin Heidelberg, Berlin, Heidelberg. [https://doi.org/10.1007/978-](https://doi.org/10.1007/978-3-642-60582-6)
489 [3-642-60582-6](https://doi.org/10.1007/978-3-642-60582-6)

490 Kimmich, R., 1977. Nuclear Magnetic Relaxation in the Presence of Quadrupole Nuclei. *Z. Für*
491 *Naturforschung A* 32, 544–554. <https://doi.org/10.1515/zna-1977-0604>

492 Korb, J.-P., 2018. Multiscale nuclear magnetic relaxation dispersion of complex liquids in bulk and
493 confinement. *Prog. Nucl. Magn. Reson. Spectrosc.* 104, 12–55.
494 <https://doi.org/10.1016/j.pnmrs.2017.11.001>

495 Larson, R.G., Van Dyk, A.K., Chatterjee, T., Ginzburg, V.V., 2022. Associative thickeners for
496 waterborne paints: Structure, characterization, rheology, and modeling. *Prog. Polym. Sci.*
497 129, 101546. <https://doi.org/10.1016/j.progpolymsci.2022.101546>

498 Laurie, A.P. (Arthur P., 1926. *The painter's methods & materials : the handling of pigments in oil,*
499 *tempera, water-colour & in mural painting, the preparation of grounds & canvas, & the*
500 *prevention of discolouration, together with the theories of light & colour applied to the*
501 *making of pictures.* London : Seeley, Service & Co. Ltd.

502 Li, Q., Berraud-Pache, R., Yang, Y., Souprayen, C., Jaber, M., 2023. Biocomposites based on bentonite
503 and lecithin: An experimental approach supported by molecular dynamics. *Appl. Clay Sci.*
504 231, 106751. <https://doi.org/10.1016/j.clay.2022.106751>

505 Luengo, C., Brigante, M., Antelo, J., Avena, M., 2006. Kinetics of phosphate adsorption on goethite:
506 Comparing batch adsorption and ATR-IR measurements. *J. Colloid Interface Sci.* 300, 511–
507 518. <https://doi.org/10.1016/j.jcis.2006.04.015>

508 Manasse, A., Mellini, M., 2006. Iron (hydr)oxide nanocrystals in raw and burnt sienna pigments. *Eur.*
509 *J. Mineral.* 18, 845–853. <https://doi.org/10.1127/0935-1221/2006/0018-0845>

510 Manea, M.M., Moise, I.V., Virgolici, M., Negut, C.D., Barbu, O.-H., Cutrubinis, M., Fugaru, V.,
511 Stanculescu, I.R., Ponta, C.C., 2012. Spectroscopic evaluation of painted layer structural
512 changes induced by gamma radiation in experimental models. *Radiat. Phys. Chem.* 81, 160–
513 167. <https://doi.org/10.1016/j.radphyschem.2011.09.015>

514 Mayer, R., Sheehan, S., 1991. *The artist's handbook of materials and techniques*, 5th ed.,
515 rev.updated. ed. Viking, New York, N.Y., U.S.A.

516 Mazzeo, R., Prati, S., Quaranta, M., Joseph, E., Kendix, E., Galeotti, M., 2008. Attenuated total
517 reflection micro FTIR characterisation of pigment–binder interaction in reconstructed paint
518 films. *Anal. Bioanal. Chem.* 392, 65–76. <https://doi.org/10.1007/s00216-008-2126-5>

519 Meilunas, R.J., Bentsen, J.G., Steinb, A., 1990. Analysis of Aged Paint Binders by FTIR Spectroscopy 20.
520 Merrifield, M.P. (Ed.), 1999. *Medieval and Renaissance treatises on the arts of painting: original texts*
521 *with English translations.* Dover Publications, Mineola, N.Y.

522 Mørup, S., Bo Madsen, M., Franck, J., Villadsen, J., Koch, C.J.W., 1983. A new interpretation of
523 Mössbauer spectra of microcrystalline goethite: “Super-ferromagnetism” or “super-spin-
524 glass” behaviour? *J. Magn. Magn. Mater.* 40, 163–174. [https://doi.org/10.1016/0304-8853\(83\)90024-0](https://doi.org/10.1016/0304-8853(83)90024-0)

525

526 Mueller, S., Llewellyn, E.W., Mader, H.M., 2010. The rheology of suspensions of solid particles. *Proc.*
527 *R. Soc. Math. Phys. Eng. Sci.* 466, 1201–1228. <https://doi.org/10.1098/rspa.2009.0445>

528 Navas, N., Romero-Pastor, J., Manzano, E., Cardell, C., 2010. Raman spectroscopic discrimination of
529 pigments and tempera paint model samples by principal component analysis on first-
530 derivative spectra. *J. Raman Spectrosc.* 41, 1486–1493. <https://doi.org/10.1002/jrs.2646>

531 Phenix, A., 1997. The composition and chemistry of eggs and egg tempera, in: *Early Italian Paintings :*
532 *Techniques and Analysis.* Maastricht, pp. 11–20.

533 Puisto, A., Illa, X., Mohtaschemi, M., Alava, M.J., 2012. Modeling the viscosity and aggregation of
534 suspensions of highly anisotropic nanoparticles. *Eur. Phys. J. E* 35, 6.
535 <https://doi.org/10.1140/epje/i2012-12006-1>

536 Romero-Pastor, J., Cardell, C., Manzano, E., Yebra-Rodríguez, Á., Navas, N., 2011. Assessment of
537 Raman microscopy coupled with principal component analysis to examine egg yolk-pigment
538 interaction based on the protein C-H stretching region (3100-2800 cm⁻¹): Multivariate
539 Raman study of egg yolk-pigment interaction. *J. Raman Spectrosc.* 42, 2137–2142.
540 <https://doi.org/10.1002/jrs.2977>

541 Salvant Plisson, J., de Viguerie, L., Tahroucht, L., Menu, M., Ducouret, G., 2014. Rheology of white
542 paints: How Van Gogh achieved his famous impasto. *Colloids Surf. Physicochem. Eng. Asp.*
543 458, 134–141. <https://doi.org/10.1016/j.colsurfa.2014.02.055>
544 Schulze, D.G., 1984. The Influence of Aluminum on Iron Oxides. VIII. Unit-Cell Dimensions of Al-
545 Substituted Goethites and Estimation of Al From Them. *Clays Clay Miner.* 32, 36–44.
546 <https://doi.org/10.1346/CCMN.1984.0320105>
547 Schwertmann, U., Carlson, L., 1994. Aluminum Influence on Iron Oxides: XVII. Unit-Cell Parameters
548 and Aluminum Substitution of Natural Goethites. *Soil Sci. Soc. Am. J.* 58, 256–261.
549 <https://doi.org/10.2136/sssaj1994.03615995005800010039x>
550 Schwertmann, U., Cornell, R.M. (Eds.), 2000. *Iron Oxides in the Laboratory: Preparation and*
551 *Characterization.* Wiley-VCH Verlag GmbH, Weinheim, Germany.
552 <https://doi.org/10.1002/9783527613229>
553 Thompson, D.V., York, L.E., 1962. *The practice of tempera painting: materials and methods,*
554 *unabridged republication of the work originally published in 1936.* ed, Dover books on art
555 *instruction, anatomy.* Dover, New York.
556 Torrent, J., 1992. Fast and Slow Phosphate Sorption by Goethite-Rich Natural Materials. *Clays Clay*
557 *Miner.* 40, 14–21. <https://doi.org/10.1346/CCMN.1992.0400103>
558 Xiao, N., Zhao, Y., Yao, Y., Wu, N., Xu, M., Du, H., Tu, Y., 2020. Biological Activities of Egg Yolk Lipids: A
559 Review. *J. Agric. Food Chem.* 68, 1948–1957. <https://doi.org/10.1021/acs.jafc.9b06616>
560 Yuan, L., Chen, L., Chen, X., Liu, R., Ge, G., 2017. *In Situ* Measurement of Surface Functional Groups
561 on Silica Nanoparticles Using Solvent Relaxation Nuclear Magnetic Resonance. *Langmuir* 33,
562 8724–8729. <https://doi.org/10.1021/acs.langmuir.7b00923>
563 Zhong, B., Stanforth, R., Wu, S., Chen, J.P., 2007. Proton interaction in phosphate adsorption onto
564 goethite. *J. Colloid Interface Sci.* 308, 40–48. <https://doi.org/10.1016/j.jcis.2006.12.055>
565